Mitigation of Quasiparticle Loss in Superconducting Qubits by Phonon Scattering

Arno Bargerbos,[1,*] Lukas Johannes Splitthoff,[1] Marta Pita-Vidal,[1] Jaap J. Wesdorp,[1] Yu Liu,[2] Peter Krogstrup,[3] Leo P. Kouwenhoven,[1] Christian Kraglund Andersen,[1] and Lukas Grünhaupt[1,†]

[1] *QuTech and Kavli Institute of Nanoscience, Delft University of Technology, Delft 2628 CJ, The Netherlands*
[2] *Center for Quantum Devices, Niels Bohr Institute, University of Copenhagen, Copenhagen 2100, Denmark*
[3] *Niels Bohr Institute, University of Copenhagen, Copenhagen 2100, Denmark*

(Received 27 July 2022; revised 12 December 2022; accepted 19 December 2022; published 6 February 2023)

Quantum error correction will be an essential ingredient in realizing fault-tolerant quantum computing. However, most correction schemes rely on the assumption that errors are sufficiently uncorrelated in space and time. In superconducting qubits, this assumption is drastically violated in the presence of ionizing radiation, which creates bursts of high-energy phonons in the substrate. These phonons can break Cooper pairs in the superconductor and, thus, create quasiparticles over large areas, consequently reducing qubit coherence across the quantum device in a correlated fashion. A potential mitigation technique is to place large volumes of normal or superconducting metal on the device, capable of reducing the phonon energy to below the superconducting gap of the qubits. To investigate the effectiveness of this method, we fabricate a quantum device with four nominally identical nanowire-based transmon qubits. On the device, half of the niobium-titanium-nitride ground plane is replaced with aluminum (Al), which has a significantly lower superconducting gap. We deterministically inject high-energy phonons into the substrate by voltage biasing a galvanically isolated Josephson junction. In the presence of the small-gap material, we find a factor of 2–5 less degradation in the injection-dependent qubit lifetimes and observe that the undesired excited qubit state population is mitigated by a similar factor. We furthermore turn the Al normal with a magnetic field, finding no change in the phonon protection. This suggests that the efficacy of the protection in our device is not limited by the size of the superconducting gap in the Al ground plane. Our results provide a promising foundation for protecting superconducting-qubit processors against correlated errors from ionizing radiation.

DOI: 10.1103/PhysRevApplied.19.024014

I. INTRODUCTION

Superconducting qubits are one of the prime candidates in the global effort toward building a quantum computer. Tremendous technological advances have been achieved over the past decade, heralding the advent of noisy intermediate-scale quantum technologies [1–3]. In order to go beyond this intermediate scale and harness the full potential of quantum computers, fault-tolerant quantum computing will be required. Remarkable progress has been made in terms of implementing error detection and correction in recent years using superconducting circuits [4–9]. A key assumption of most quantum error-correction schemes is that qubit errors are spatially and temporally uncorrelated; however, that appears to be drastically violated in large-scale superconducting-qubit arrays. In Ref. [10] it has been shown that cosmic rays and ambient radioactivity can deposit large amounts of energy into the substrate of the device in the form of phonons. These phonons travel over distances of centimeters, breaking up Cooper pairs and leading to decreased qubit coherence over time scales of milliseconds, causing correlated error events [10–16].

Several mitigation strategies have been proposed to combat these ionizing impact events at the level of the quantum device, such as the direct trapping of quasiparticles through gap engineering [17–20] as well as impeding the propagation of phonons by substrate modification [21–24]. A complementary approach is the use of so-called phonon traps [15,23,25–27]. Made from a normal or superconducting material with a small superconducting gap, phonon traps dissipate the phonon energy through scattering events until the resulting phonons have too little energy to break Cooper pairs in the qubit layer. A key difference of phonon traps compared to the direct trapping of quasiparticles is that the traps also target the phonons while they are en route to the qubits, before error events occur. Furthermore, phonon traps do not have to be galvanically connected to the circuit; nor do they even have to be embedded into the same plane of the chip, as long as

*a.bargerbos@tudelft.nl
†Now at Physikalisch-Technische Bundesanstalt, 38116 Braunschweig, Germany; lukas.gruenhaupt@ptb.de

they connect to the substrate. It is therefore possible to design phonon traps without introducing qubit dissipation from coupling to lossy materials [19] and with no added strain on the increasingly complex task of control-line routing [28].

II. DEVICE

To date, the efficacy of phonon traps has been demonstrated for superconducting resonators [25,26] and kinetic inductance detectors [23]. In this paper, we set out to investigate their effectiveness in protecting superconducting qubits by fabricating a 6×6 mm^2 chip containing four nanowire transmon qubits [29,30], one in each corner of the device [Fig. 1(a)]. All transmons have identical geometries [Fig. 1(b)] and are excited and read out via individual coplanar waveguide resonators coupled to a common feed line. The transmon islands, resonators, and feed line are dry etched from a 20-nm-thick niobium-titanium-nitride (Nb-Ti-N) thin film deposited on a 525-μm-thick high-resistivity silicon substrate. We implement the phonon traps by partially removing the Nb-Ti-N ground plane on one half of the chip and replacing it with 200 nm of aluminum (Al) deposited by electron-beam evaporation and patterned by lift-off [cf. Fig. 1(e)]. Furthermore, the Al and Nb-Ti-N layers are galvanically connected by a 20-μm-wide region of overlap between them. We leave a 290-μm region of Nb-Ti-N around all qubit islands to suppress direct quasiparticle trapping in the Al layer surrounding the qubit [18,19]. While quasiparticle trapping can be of great use in practical qubit applications, the goal of this study is to evaluate the effect of phonon trapping only. Finally, the full backside of the chip is glued to a solid copper block using thermally conductive silver epoxy. Through the copper, the chip and surrounding enclosure are thermally anchored to the mixing chamber of a dilution refrigerator at approximately 20 mK.

Each transmon island is connected to ground via a nominally 10-μm-long epitaxial semiconductor-superconductor nanowire, consisting of a 110-nm-wide hexagonal InAs core and a 6-nm-thick Al shell covering two of its facets [31]. By selectively removing a 100-nm-long segment from the Al shell, we define a semiconducting Josephson junction, the Josephson energy of which can be tuned with a single bottom-gate electrode via the field effect [29,30]. A second gate electrode is present under an InAs-Al region of the nanowire, allowing for capacitive tuning of the offset charge of the island and aiding in the estimation of the qubit parameters (see the Supplemental Material [32]). The choice of nanowire-based junctions over conventional tunnel junctions is motivated by their magnetic field compatibility [33–35], allowing us to study the dependence of the phonon-trapping efficacy on the size of the superconducting gap in the 200-nm-thick Al ground plane

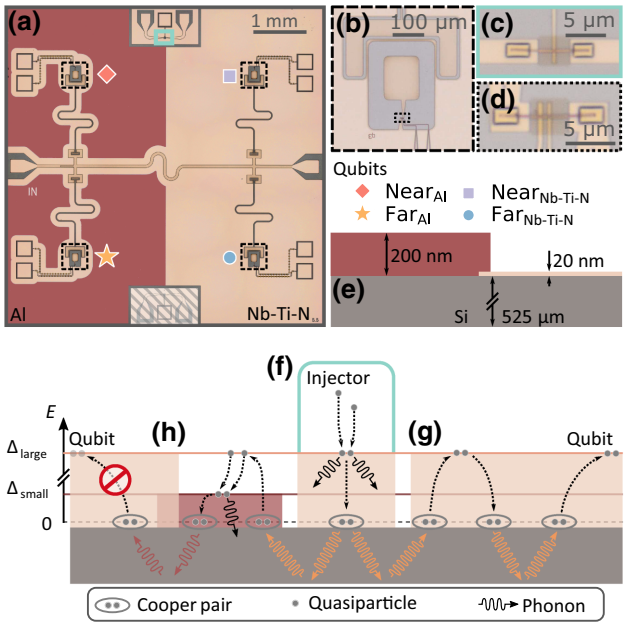

FIG. 1. A false-colored (a)–(e) device overview and (f)–(h) sketch of the phonon mitigation process. (a) Four nanowire transmon qubits [(b), dashed boxes] are coupled to individual readout resonators, which in turn are coupled to a common feed line. Two nanowire-based junctions are additionally present for phonon injection [(c), turquoise boxes] and are galvanically isolated from the qubit ground plane (bottom junction not operational). All structures are patterned from Nb-Ti-N (light orange), except for the majority of the left half of the ground plane, which is made from a thick aluminum film (red) [see the device cross section in (e); lateral dimension not to scale]. Electrostatic gates below the junctions tune the resistance of (c) the phonon injector and (d) the Josephson energy of the qubits [an enlargement of (b)], respectively. A second gate per qubit allows for independent tuning of the qubit charge offsets. (f) Quasiparticles excited by voltage biasing of the injector relax to the superconducting gap edge and recombine, emitting phonons (black and orange arrows, respectively). (g) The emitted phonons propagate via the substrate and those with energies larger than twice the superconducting gap $> 2\Delta_{large}$ induce Cooper-pair breaking, relaxation, and recombination cycles, eventually exciting quasiparticles in the qubits. (h) In the presence of a small-gap superconductor, these cycles produce phonons of energy $\leq 2\Delta_{small}$ instead (red arrows), which cannot break Cooper pairs in the qubits.

without strongly affecting the qubit parameters (see the Supplemental Material [32]).

A key feature of our device is two additional semiconducting junctions used for phonon injection. Identical to those used for the transmons, the junctions are located at the top and bottom of the front side of the chip but are galvanically isolated from the qubit ground plane [see Fig. 1(a)]. They are connected to source and drain leads made from the Nb-Ti-N base layer to allow for voltage biasing and current sensing, while the resistance of the junctions can be tuned with a bottom-gate electrode (see

the Supplemental Material [32]). In this paper, only the top junction is used, as the bottom junction is not functional. Given that the four qubits can be uniquely identified based on their distance from the top junction (1.8 mm or 4.4 mm; see the Supplemental Material [32]) and whether their ground plane is made from Al or Nb-Ti-N, in what follows we label them as the Near_{Al}, $\text{Near}_{\text{Nb-Ti-N}}$, Far_{Al}, and $\text{Far}_{\text{Nb-Ti-N}}$ qubits.

The top junction serves to inject phonons over a broad spectral distribution up to energies $\leq eV_{\text{bias}} - 2\Delta_{\text{nw}}$ into the substrate of the chip, where Δ_{nw} is the superconducting gap of the injector junction [36]. This technique originates in the investigation of nonequilibrium phonon dynamics [37–39] and has more recently been adapted for experiments involving superconducting quantum circuits [25,40,41]. The purpose of the injection junction is to qualitatively reproduce the phonon spectrum present several microseconds after a cosmic ray impact event. By virtue of the phononic dispersion relation and interactions with the superconducting layers, at this stage most of the energy will have been converted into phonons with a broad energy spectrum ranging up to several millielectronvolts [15], similar to the spectrum resulting from the phonon injection by voltage biasing a Josephson junction. However, the total energy of an impact event, ranging up to megaelectronvolt scales, remains difficult to experimentally generate using Josephson junctions [15,36].

III. PHONON INJECTION AND PROPAGATION

As the phonon injection and propagation process is central to this experiment, we briefly discuss the operation mechanism here and it is visually represented in Figs. 1(f)–1(h). We set the bottom-gate voltage of the junction such that we operate in the tunneling regime, where the supercurrent at bias voltage, $V_{\text{bias}} = 0$, is fully suppressed (see the Supplemental Material [32]). For voltages $V_{\text{bias}} < |2\Delta_{\text{nw}}|/e$ applied between the leads of the junction, there is thus no current, where Δ_{nw} is the superconducting gap of the InAs-Al nanowires. However, for voltages $V_{\text{bias}} \geq |2\Delta_{\text{nw}}|/e$, Cooper pairs can be broken up and a quasiparticle current will run across the junction [see Fig. 2(a)]. The quasiparticles then diffuse around the vicinity of the junction and its leads, scattering and relaxing to the gap edge of the superconductors, producing relaxation phonons of energies up to $E = eV_{\text{bias}} - \Delta_{\text{nw}}$ in the process [see Fig. 1(f) and Ref. [36]]. The now-relaxed quasiparticles can subsequently also recombine with other quasiparticles, emitting recombination phonons of energy $E = 2\Delta_{\text{nw}}$ [42]. These phonons either break up new Cooper pairs in the metal layer or they escape into the substrate, where they can rapidly travel over distances of several times the size of the chip, scattering off the boundaries [43]. The phonons can thus end up at the qubits, creating quasiparticles and inducing losses

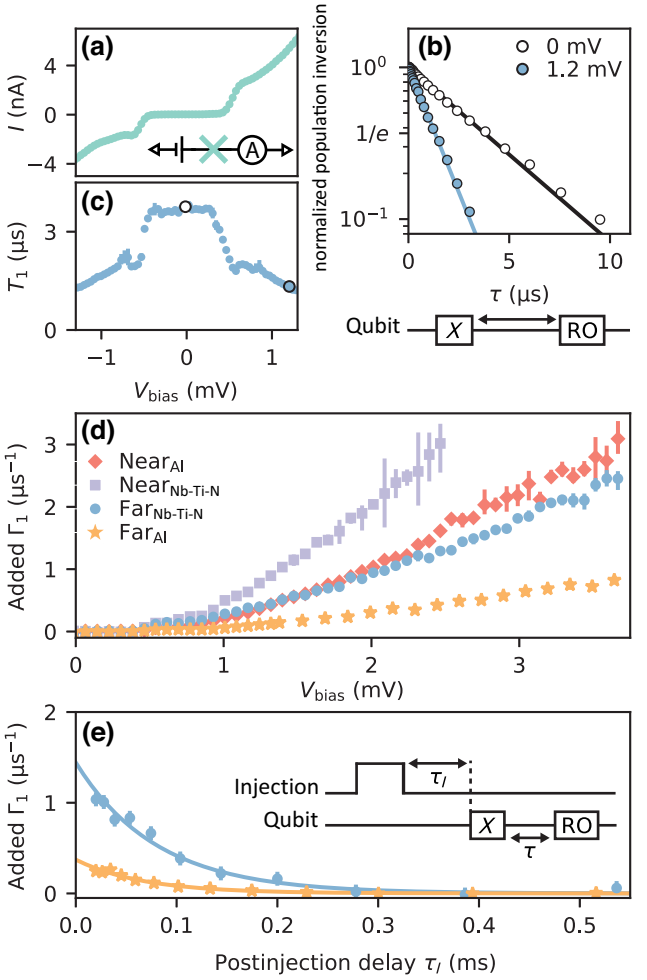

FIG. 2. The added-qubit-loss due to phonon injection. (a) The current-voltage (I-V) characteristics of the Josephson junction used to inject phonons measured using the circuit shown in the inset. The "A" denotes a current meter. (b) Representative qubit-lifetime (T_1) measurements on the $\text{Far}_{\text{Nb-Ti-N}}$ qubit for bias voltages V_{bias} of 0 and 1.2 mV applied across the injector. The data (markers) are fitted with an exponential decay (solid lines), yielding lifetimes of 3.8 μs and 1.3 μs, respectively. In the pulse sequence X denotes the pulse to excite the qubit, while RO indicates the readout pulse. (c) The qubit lifetime T_1 of the $\text{Far}_{\text{Nb-Ti-N}}$ qubit as a function of V_{bias}. (d) The added-qubit-loss rate Γ_1 as a function of V_{bias} for all four qubits (the labels apply to all panels). We define the added Γ_1 as the bias-voltage-dependent loss rate minus the average baseline value for $|eV_{\text{bias}}| < 2\Delta_{\text{nw}}$ [cf. (c)]. (e) The added Γ_1 as a function of the delay time τ_I after a square injection pulse with a duration of 20 μs and an amplitude of approximately 3 mV. The loss rates are fitted with an exponential decay (solid line), yielding recovery times of 80 ± 9 μs (blue) and 67 ± 5 μs (orange). The error bars in (c)–(e) denote the standard deviation over five repetitions.

proportional to the excess quasiparticle density x_{qp} [44] [see Fig. 1(h)]. However, if the phonons encounter the Al traps en route to the qubits, part of their energy can be dissipated in further cycles of Cooper pair breaking,

relaxation, and recombination [Fig. 1(g)]. The resulting phonons of energy $E \leq 2\Delta_{\text{trap}}$ can no longer excite quasiparticles in the qubit structures, for which the superconducting gaps of the islands, $\Delta_{\text{Nb-Ti-N}} \geq 1500$ μeV, and of the nanowires $\Delta_{\text{nw}} = 270$ μeV are larger than that of the traps $\Delta_{\text{trap}} = 180$ μeV (see Refs. [45–47]; see also the Supplemental Material [32]).

We note that at cryogenic temperatures, phonons move through the silicon substrate virtually unimpeded with a velocity of approximately 6 mm μs^{-1} and thus traverse the chip on microsecond time scales. Additionally, we expect the scattering length of phonons in the Al film to be comparable to the thickness of the Al trapping region, such that they have a significant probability of escaping from the film without creating quasiparticles [15]. Thus, we anticipate the phonons to be able to fully traverse the chip, with the main impediments to their propagation coming from the probability of scattering into quasiparticles and from the probability of escaping through the silver epoxy on the backside of the sample. However, accurate modeling of the phonon distribution in the substrate would critically rely on phonon-transfer rates through the various interfaces, the scattering lengths in the different materials, and adequate numerical simulations of the phonon propagation trajectories (cf. Ref. [43]).

IV. MITIGATION OF LOSS DUE TO PHONON INDUCED QUASIPARTICLES

To investigate the effectiveness of the Al ground plane to protect against high-energy phonons, we perform qubit lifetime (T_1) experiments on all four qubits while we apply a constant bias to the phonon injector, which causes the T_1 time to decrease as shown in Fig. 2(b). For bias voltages within the gap, T_1 remains essentially constant [see Fig. 2(c)], while T_1 decreases drastically at the onset of the quasiparticle current, with a kink at $2\Delta_{\text{nw}}$ originating from the enhanced conductance at the gap edge (see the Supplemental Material [32]). As the qubit is over 4 mm away from the galvanically isolated injector junction, this suggests that the losses indeed originate from phonons that have traveled through the substrate [25]. We then compare the added loss rate $\Gamma_1(V_{\text{bias}}) = 1/T_1(V_{\text{bias}}) - 1/T_1(V_{\text{bias}} < |2\Delta_{\text{nw}}/e|)$ of each qubit, where we subtract the baseline loss rate measured inside the superconducting gap. As can be seen in Fig. 2(d), the Far_{Al} qubit has an up to 8 times smaller added loss rate than the $\text{Near}_{\text{Nb-Ti-N}}$ qubit. However, this comparison involves both a larger separation from the injector and the presence of phonon traps. To disentangle the two effects, we compare the qubits at equal distance from the injector. The Near_{Al} qubit has an up to 2.5 times smaller added loss rate than the $\text{Near}_{\text{Nb-Ti-N}}$ qubit, supporting the notion that the presence of the Al phonon traps leads to resilience against phonon-induced losses. For the $\text{Far}_{\text{Nb-Ti-N}}$ and Far_{Al} qubits, the improvement even reaches up to a factor of 5, suggesting that an increased area of the trapping region increases the efficacy (see the Supplemental Material [32]). We note that the improvements are bias dependent, tending toward a constant value for bias voltages above 1.5 mV, several times the size of Δ_{nw}.

So far, we have focused on phonons that are continuously injected into the chip by applying a constant bias voltage across the injector. However, in the impact events of ionizing radiation, the phonons are created in bursts. To test whether our findings still hold under such circumstances, we repeat the same experiment using a pulsed phonon-injection scheme. We now apply a square pulse of duration 20 μs at an amplitude of approximately 3 mV across the injector. This would result in an energy of approximately 5 keV if all energy was transduced into phonons—about 2 orders of magnitude smaller than during a typical high-energy particle impact but with a spectrum similar to that some microseconds after the initial impact [15,36]. Subsequently, we measure the qubit loss as a function of the delay time after the injection event [Fig. 2(e)]. The recovery of the added loss rate with the delay time follows an exponential form, suggesting a recovery dominated by quasiparticle relaxation rather than by recombination, for which the recovery is governed by a hyperbolic cotangent function [17]. We find that at zero delay time, the $\text{Far}_{\text{Nb-Ti-N}}$ qubit is affected 4 times more than the Far_{Al} qubit, consistent with the results for continuous injection. We further note that the recovery times are approximately equal at 80 ± 9 μs [67 ± 5 μs] for the $\text{Far}_{\text{Nb-Ti-N}}$ [Far_{Al}] qubit. We do not observe any significant enhancement of the recovery time due to the presence of the Al phonon traps, so the recovery time might instead be dominated by quasiparticle dynamics near the junction, such as quasiparticle trapping and diffusion rates. The latter could be addressed with quasiparticle traps rather than with phonon traps [18,19]. Alternatively, the phonon traps could have a similar effect on recovery times across the device, as the phonons can traverse the chip on time scales of a few microseconds [15]. We note that the time scale for phonons to leave the chip is also several microseconds and this is therefore unlikely to be the limiting mechanism of the observed recovery time.

V. INCREASED EXCITED-STATE POPULATION DUE TO PHONON INJECTION

In the measurements of the qubit loss rates, we additionally find that the qubit readout signal becomes smaller with increasing bias voltages, requiring substantially more repetitions to obtain the same signal-to-noise ratio (SNR) at elevated bias. To investigate this effect, we monitor the resonator response of the $\text{Far}_{\text{Nb-Ti-N}}$ qubit using single-shot readout in the absence of any qubit-excitation tones. For 0-mV bias, this results in a double Gaussian distribution of

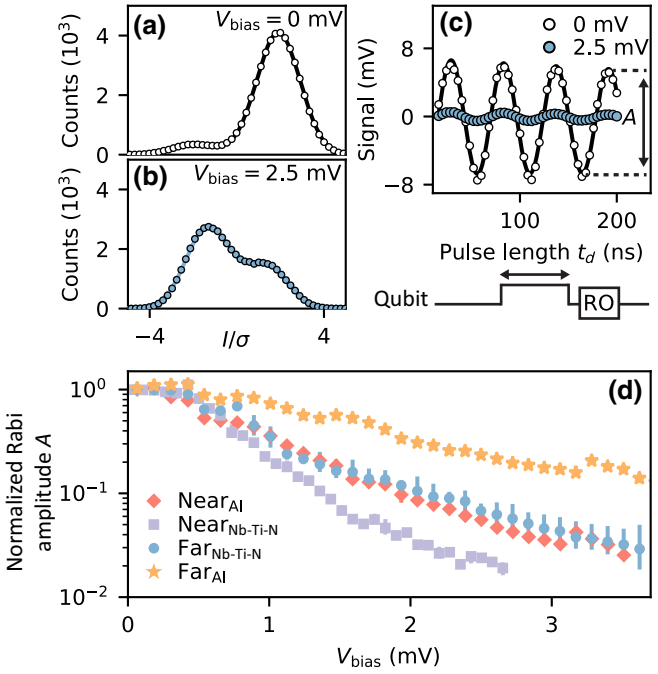

FIG. 3. The increased excited-state population due to phonon injection. (a) A histogram of the resonator response for the $\text{Far}_{\text{Nb-Ti-N}}$ qubit at $V_{\text{bias}} = 0$ mV. Each individual shot corresponds to the integrated output signal for a readout time of 500 ns. The resulting histogram (markers) is fitted with a double Gaussian function (solid line), from which we estimate a ground-state population of 93%. (b) The same as (a) but for $V_{\text{bias}} = 2.5$ mV, from which we estimate a ground-state population of 35%. (c) Representative time-Rabi experiments on the $\text{Far}_{\text{Nb-Ti-N}}$ qubit for the values of V_{bias} used in (a) and (b). The data (markers) are fitted with an exponentially decaying cosine (solid line). (d) The extracted Rabi-oscillation amplitude A normalized to its value at zero bias, measured as a function of V_{bias} for all four qubits. The error bars in (d) denote the standard deviation over five repetitions.

measurement outcomes, with 93% of the outcomes located in a single Gaussian [Fig. 3(a)]. We interpret this output as the signal corresponding to the ground-state population of the transmon qubit, indicating a residual excited-state population of 7%. When we apply a constant bias of 2.5 mV, the distribution changes significantly: the transmon is now in the ground state only 35% of the time. This is consistent with previous findings showing that nonequilibrium quasiparticles with energies in excess of $2\Delta_{\text{nw}}$ can lead to an increased excited-state population [41,48,49]. Furthermore, the fact that the ground-state population is less than 50% could indicate that the transmon now also has a sizable population outside of the two-level qubit subspace and that nonequilibrium quasiparticles resulting from high-energy phonons can thus also cause qubit leakage errors, which are not easily mitigated in standard error-correction schemes [50,51]. However, the SNR of our measurements is not large enough to distinguish the different excited transmon states; in particular, for elevated bias voltages that strongly reduce the qubit lifetime as well as potentially populate a plethora of states.

To gain insight into the effectiveness of the traps in reducing the unwanted excited population, while constrained by limited SNR, we perform a time-Rabi experiment between the ground and first excited state of the transmons as a function of the injection bias voltage. The amplitude of the Rabi oscillation A is proportional to the difference in the population of the transmon states involved and, additionally, decreases in the presence of qubit leakage. The evolution of A with V_{bias} is thus indicative of the change in the state populations. As shown in Fig. 3(c), the amplitude of the oscillations for the $\text{Far}_{\text{Nb-Ti-N}}$ qubit indeed decreases significantly at $V_{\text{bias}} = 2.5$ mV compared to that at 0 mV. We repeat this experiment for all qubits, normalizing the Rabi amplitude to its value at zero injection voltage. We find results comparable to those of the added-qubit-loss-rates, with the Near_{Al} qubit again showing a reduction in Rabi amplitude of up to 5 times more than that of the $\text{Far}_{\text{Nb-Ti-N}}$ qubit. This difference indicates that phonon traps can thus also serve to reduce the unwanted excited-state population induced by the generation of nonequilibrium quasiparticles by phonons. We note that such energetic quasiparticles are likely only produced during the initial phase following an impact event [10,15], while they are constantly observed in this experiment due to the continuous injection of high-energy phonons.

VI. SUPERCONDUCTING vs. NORMAL CONDUCTING PHONON TRAP

Having established moderate protection due to the Al traps, we investigate how the difference in the superconducting gap between the trapping and qubit materials influences the effectiveness of the trapping process. For the trapping process to be of use, the superconducting gap of the trap must be smaller than that of the qubit layer [cf. Figs. 2(f)–2(h)]. Furthermore, as the relaxation rate of quasiparticles excited inside the trap grows with their energy above the gap edge [19,52], one would assume that the absolute size of gap should also be a relevant metric. Ignoring potentially detrimental effects from electromagnetic coupling, a normal metal (with no spectral gap) might thus be particularly suitable as a trapping material [15,25]. We investigate this hypothesis *in situ*, making use of the inherent magnetic field compatibility of the nanowire transmon qubits and their readout circuit, which have been shown to be operable up to parallel fields in excess of 1 T [33–35,53]. This is in contrast to the 200-nm-thick Al, which turns normal at significantly lower fields of approximately 30 mT [see Fig. 4(b) and Ref. [54]].

We repeat the measurements of the added loss rate in the presence of a constant bias voltage for different applied

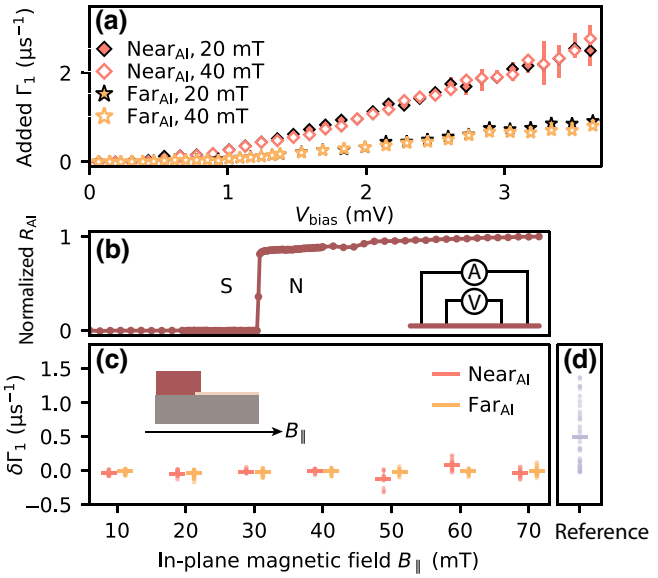

FIG. 4. The magnetic field independence of the added-qubit-loss. (a) The added Γ_1 as a function of V_{bias} for the two qubits with an aluminum ground plane at magnetic fields $B_\parallel$ of 20 and 40 mT applied in the plane of the chip [cf. (c), inset]. (b) The four-point measurement of the normalized aluminum film resistance R_{Al} as a function of $B_\parallel$. The "A" denotes a current meter and "V" denotes a voltmeter. (c) A scatter plot showing the differences between the V_{bias} dependence of Γ_1 at zero and elevated $B_\parallel$ for the two qubits with an aluminum ground plane. Each data point represents the difference in rates $\delta\Gamma_1$ evaluated at equal V_{bias}. The horizontal line indicates the mean of $\delta\Gamma_1$ over all V_{bias}. The inset shows the direction of the applied magnetic field with respect to the cross section of the chip. (d) The same type of plot as (c) but showing the difference between the Near_{Al} and $\text{Near}_{Nb\text{-}Ti\text{-}N}$ qubits at zero applied magnetic field [data shown in Fig. 2(d)]. This serves as a reference for the data in (c).

magnetic fields. Contrary to expectations, the added loss rate does not appear to change after passing the critical parallel field of the thick Al [Fig. 4(a)]. In fact, we do not detect any significant change as a function of magnetic field between 0 and 70 mT, far in excess of the critical field [Fig. 4(c)]. To elucidate the implications of these findings, we conservatively estimate the relaxation rate of quasiparticles at energy $2\Delta_{nw}$ to be at least 30% faster in normal-state Al than in zero-field superconducting Al due to the reduction in the gap size [19]. Given that despite this no improvement is observed, we conclude that the rate at which excited quasiparticles relax inside the phonon trap is not what sets the effectiveness of our phonon traps.

We instead consider that the bottleneck for the trapping efficacy is the rate at which phonons are able to scatter and excite quasiparticles in the trapping layer. This rate has two primary components: the scattering rate of phonons into quasiparticles inside the Al and the transmission probability for phonons to cross from the silicon substrate into the Al. The first component is predicted to decrease moderately when entering the normal state [15]; a negative change in trapping efficacy would thus have been observed if this was the limiting factor. The second component, the transmission probability, is not expected to be a function of the field. Consequently, we hypothesize that the trapping is limited by the poor interface between the substrate and the Al layer [43,55], making it difficult for phonons to enter the traps. In our device, this is potentially exacerbated by the dry-etching procedure used to remove the Nb-Ti-N layer before Al deposition, which roughens the underlying silicon, reducing phonon transmission across the metal-substrate interface. We again note that the magnetic field experiment is performed using continuous injection rather than using pulsed injection. Potential improvements during the phase where most phonons are reduced to energies of $2\Delta_{nw}$ might thus be obfuscated by the constant influx of new high-energy phonons.

VII. CONCLUSION

In conclusion, we find a factor of 2–5 improvement in the protection against phonon-induced degradation of qubit lifetimes for transmon qubits surrounded by Al phonon traps. This level of improvement is in line with previous results on phonon trapping for superconducting resonators [25,26] and kinetic inductance detectors [23], here demonstrated at the level of sensitivity of transmon qubits. Additionally, we demonstrate that phonon traps can also be used to combat the increase in the excited-state population due to the generation of energetic quasiparticles from phonons. While the obtained improvements are modest, we emphasize that this is a conservative estimate for realistic multiqubit arrays. With mean free paths exceeding several times the size of the chip, phonons in the silicon are able to travel vast distances and thus it is likely that the two Nb-Ti-N–based qubits also benefit from the presence of the Al traps. Therefore, we believe that the improvement found is a lower bound on what could be obtained when comparing different chips with and without traps, which we choose not to do to exclude unintended differences between devices and thermal anchoring of the respective chips. Furthermore, we deliberately thermally anchor the full backside of the chip, allowing phonons to leave the device via the substrate. This is in contrast to most superconducting-qubit implementations, where the chips are mounted in a floating configuration [15,56,57]. In these devices, the main path for the phonons to escape the device is through the wire bonds at the perimeter of the chip, a slow process that enhances the probability of the phonons interacting with the traps in such devices.

Finally, we highlight the fact that phonon traps are also relevant for transmons realized with conventional Al-AlO_x-Al Josephson junctions [46], as well as for other types of superconducting qubits, such as fluxoniums [59] and novel protected qubit designs [60]. The enhanced

rates of quasiparticle poisoning events following an impact event are also expected to be highly detrimental for parity-based qubits such as Andreev qubits [61,62], as well as for topologically protected Majorana qubits [63,64]. The current generation of devices used in these qubit platforms relies on the same type of superconductor-semiconductor nanowires as used in this experiment. Furthermore, while not directly sensitive to superconductor-based quasiparticles, spin qubits are known to suffer phonon-mediated back action [65,66] and might also suffer from correlated errors due to phonon impacts, although to what extent remains to be investigated.

The data and analysis code that support the findings of this study are openly available in 4TU.ResearchData [75].

ACKNOWLEDGMENTS

We gratefully acknowledge Olaf Benningshof, Jason Mensingh, and Raymond Schouten for technical support. We further thank Grzegorz Mazur for help with the critical field measurements, Gianluigi Catelani for discussions about quasiparticle dynamics, and Bernard van Heck, Ruben ter Meulen, Daniele Piras, and Delphine Brousse for fruitful exchanges. This research is cofunded by the allowance for Top consortia for Knowledge and Innovation (TKIs) from the Dutch Ministry of Economic Affairs, research project "Scalable circuits of Majorana qubits with topological protection" (i39, SCMQ) with project number 14SCMQ02, from the Dutch Research Council (NWO) and the Microsoft Quantum initiative. C.K.A. additionally acknowledges support from the Dutch Research Council (NWO).

A.B. and L.G. conceived the experiment. Y.L. and P.K. developed and provided the nanowire materials. A.B., M.P.V., L.J.S., J.J.W, C.K.A., and L.G. prepared the experimental setup and data-acquisition tools. A.B., L.J.S., M.P.V., and L.G. designed and fabricated the device. A.B. and L.G. performed the measurements and analyzed the data, with continuous feedback from L.J.S., M.P.V., J.J.W, L.P.K., and C.K.A. A.B. and L.G. wrote the manuscript, with feedback from all authors.

Note added.—Recently, we have become aware of a similar experiment by Iaia *et al.* [58]. In their work, the authors compare the impact of high-energy phonons on two separate transmon chips, where one chip has a 10-μm-thick Cu film deposited on its backside. For the Cu-covered device, they find a reduction in phonon-induced qubit errors by more than a factor of 20. These findings strongly complement the results of this paper, where we instead investigate the effect of superconducting traps. Furthermore, by comparing transmons on a single chip, we provide a conservative measure of the trapping efficacy that can be achieved. Together, these works show that phonon traps offer a promising path toward reducing correlated errors to below the level required for fault-tolerant operation.

[1] J. Preskill, Quantum computing in the NISQ era and beyond, Quantum **2**, 79 (2018).
[2] F. Arute, *et al.*, Quantum supremacy using a programmable superconducting processor, Nature **574**, 505 (2019).
[3] M. Kjaergaard, M. E. Schwartz, J. Braumüller, P. Krantz, J. I.-J. Wang, S. Gustavsson, and W. D. Oliver, Superconducting qubits: Current state of play, Annu. Rev. Condens. Matter Phys. **11**, 369 (2020).
[4] C. K. Andersen, A. Remm, S. Lazar, S. Krinner, N. Lacroix, G. J. Norris, M. Gabureac, C. Eichler, and A. Wallraff, Repeated quantum error detection in a surface code, Nat. Phys. **16**, 875 (2020).
[5] Z. Chen, *et al.*, Exponential suppression of bit or phase errors with cyclic error correction, Nature **595**, 383 (2021).
[6] J. F. Marques, B. M. Varbanov, M. S. Moreira, H. Ali, N. Muthusubramanian, C. Zachariadis, F. Battistel, M. Beekman, N. Haider, W. Vlothuizen, A. Bruno, B. M. Terhal, and L. DiCarlo, Logical-qubit operations in an error-detecting surface code, Nat. Phys. **18**, 80 (2021).
[7] S. Krinner, N. Lacroix, A. Remm, A. D. Paolo, E. Genois, C. Leroux, C. Hellings, S. Lazar, F. Swiadek, J. Herrmann, G. J. Norris, C. K. Andersen, M. Müller, A. Blais, C. Eichler, and A. Wallraff, Realizing repeated quantum error correction in a distance-three surface code, Nature **605**, 669 (2022).
[8] N. Sundaresan, T. J. Yoder, Y. Kim, M. Li, E. H. Chen, G. Harper, T. Thorbeck, A. W. Cross, A. D. Córcoles, and M. Takita, Matching and maximum likelihood decoding of a multi-round subsystem quantum error correction experiment, arXiv e-prints (2022), ArXiv:2203.07205.
[9] R. Acharya, *et al.*, Suppressing quantum errors by scaling a surface code logical qubit, arXiv e-prints (2022), ArXiv:2207.06431.
[10] M. McEwen, *et al.*, Resolving catastrophic error bursts from cosmic rays in large arrays of superconducting qubits, Nat. Phys. **18**, 107 (2021).
[11] L. J. Swenson, A. Cruciani, A. Benoit, M. Roesch, C. S. Yung, A. Bideaud, and A. Monfardini, High-speed phonon imaging using frequency-multiplexed kinetic inductance detectors, Appl. Phys. Lett. **96**, 263511 (2010).
[12] D. C. Moore, S. R. Golwala, B. Bumble, B. Cornell, P. K. Day, H. G. LeDuc, and J. Zmuidzinas, Position and energy-resolved particle detection using phonon-mediated microwave kinetic inductance detectors, Appl. Phys. Lett. **100**, 232601 (2012).
[13] A. P. Vepsäläinen, A. H. Karamlou, J. L. Orrell, A. S. Dogra, B. Loer, F. Vasconcelos, D. K. Kim, A. J. Melville, B. M. Niedzielski, J. L. Yoder, S. Gustavsson, J. A. Formaggio, B. A. VanDevender, and W. D. Oliver, Impact of ionizing radiation on superconducting qubit coherence, Nature **584**, 551 (2020).
[14] C. D. Wilen, S. Abdullah, N. A. Kurinsky, C. Stanford, L. Cardani, G. D'Imperio, C. Tomei, L. Faoro, L. B. Ioffe, C. H. Liu, A. Opremcak, B. G. Christensen, J. L. DuBois, and R. McDermott, Correlated charge noise and relaxation

errors in superconducting qubits, Nature **594**, 369 (2021).
[15] J. M. Martinis, Saving superconducting quantum processors from decay and correlated errors generated by gamma and cosmic rays, npj Quantum Inf. **7**, 90 (2021).
[16] L. Cardani, *et al.*, Reducing the impact of radioactivity on quantum circuits in a deep-underground facility, Nat. Commun. **12**, 2773 (2021).
[17] C. Wang, Y. Y. Gao, I. M. Pop, U. Vool, C. Axline, T. Brecht, R. W. Heeres, L. Frunzio, M. H. Devoret, G. Catelani, L. I. Glazman, and R. J. Schoelkopf, Measurement and control of quasiparticle dynamics in a superconducting qubit, Nat. Commun. **5**, 5836 (2014).
[18] R.-P. Riwar, A. Hosseinkhani, L. D. Burkhart, Y. Y. Gao, R. J. Schoelkopf, L. I. Glazman, and G. Catelani, Normal-metal quasiparticle traps for superconducting qubits, Phys. Rev. B **94**, 104516 (2016).
[19] R.-P. Riwar and G. Catelani, Efficient quasiparticle traps with low dissipation through gap engineering, Phys. Rev. B **100**, 144514 (2019).
[20] X. Pan, Y. Zhou, H. Yuan, L. Nie, W. Wei, L. Zhang, J. Li, S. Liu, Z. H. Jiang, G. Catelani, L. Hu, F. Yan, and D. Yu, Engineering Superconducting Qubits to Reduce Quasiparticles and Charge Noise, Nat. Commun. **13**, 7196 (2022).
[21] Y. Chu, C. Axline, C. Wang, T. Brecht, Y. Y. Gao, L. Frunzio, and R. J. Schoelkopf, Suspending superconducting qubits by silicon micromachining, Appl. Phys. Lett. **109**, 112601 (2016).
[22] K. Rostem, P. J. de Visser, and E. J. Wollack, Enhanced quasiparticle lifetime in a superconductor by selective blocking of recombination phonons with a phononic crystal, Phys. Rev. B **98**, 014522 (2018).
[23] K. Karatsu, A. Endo, J. Bueno, P. J. de Visser, R. Barends, D. J. Thoen, V. Murugesan, N. Tomita, and J. J. A. Baselmans, Mitigation of cosmic ray effect on microwave kinetic inductance detector arrays, Appl. Phys. Lett. **114**, 032601 (2019).
[24] T. A. Puurtinen, K. Rostem, P. J. de Visser, and I. J. Maasilta, A composite phononic crystal design for quasiparticle lifetime enhancement in kinetic inductance detectors, J. Low Temp. Phys. **199**, 577 (2020).
[25] U. Patel, I. V. Pechenezhskiy, B. L. T. Plourde, M. G. Vavilov, and R. McDermott, Phonon-mediated quasiparticle poisoning of superconducting microwave resonators, Phys. Rev. B **96**, 220501 (2017).
[26] F. Henriques, F. Valenti, T. Charpentier, M. Lagoin, C. Gouriou, M. Martínez, L. Cardani, M. Vignati, L. Grünhaupt, D. Gusenkova, J. Ferrero, S. T. Skacel, W. Wernsdorfer, A. V. Ustinov, G. Catelani, O. Sander, and I. M. Pop, Phonon traps reduce the quasiparticle density in superconducting circuits, Appl. Phys. Lett. **115**, 212601 (2019).
[27] P. J. de Visser, S. A. de Rooij, V. Murugesan, D. J. Thoen, and J. J. Baselmans, Phonon-Trapping-Enhanced Energy Resolution in Superconducting Single-Photon Detectors, Phys. Rev. Appl. **16**, 034051 (2021).
[28] T. Brecht, W. Pfaff, C. Wang, Y. Chu, L. Frunzio, M. H. Devoret, and R. J. Schoelkopf, Multilayer microwave integrated quantum circuits for scalable quantum computing, npj Quantum Inf. **2**, 16002 (2016).
[29] G. de Lange, B. van Heck, A. Bruno, D. J. van Woerkom, A. Geresdi, S. R. Plissard, E. P. A. M. Bakkers, A. R. Akhmerov, and L. DiCarlo, Realization of Microwave Quantum Circuits Using Hybrid Superconducting-Semiconducting Nanowire Josephson Elements, Phys. Rev. Lett. **115**, 127002 (2015).
[30] T. W. Larsen, K. D. Petersson, F. Kuemmeth, T. S. Jespersen, P. Krogstrup, J. Nygård, and C. M. Marcus, Semiconductor-Nanowire-Based Superconducting Qubit, Phys. Rev. Lett. **115**, 127001 (2015).
[31] P. Krogstrup, N. L. B. Ziino, W. Chang, S. M. Albrecht, M. H. Madsen, E. Johnson, J. Nygård, C. Marcus, and T. S. Jespersen, Epitaxy of semiconductor-superconductor nanowires, Nat. Mater. **14**, 400 (2015).
[32] See the Supplemental Material at http://link.aps.org/supplemental/10.1103/PhysRevApplied.19.024014, which contains further details about device fabrication, the experimental setup, the device tune-up, the ratios of the added loss rates, and the magnetic field dependence of the qubit frequencies. It includes Refs. [67–74].
[33] F. Luthi, T. Stavenga, O. W. Enzing, A. Bruno, C. Dickel, N. K. Langford, M. A. Rol, T. S. Jespersen, J. Nygård, P. Krogstrup, and L. DiCarlo, Evolution of Nanowire Transmon Qubits and their Coherence in a Magnetic Field, Phys. Rev. Lett. **120**, 100502 (2018).
[34] M. Pita-Vidal, A. Bargerbos, C.-K. Yang, D. J. van Woerkom, W. Pfaff, N. Haider, P. Krogstrup, L. P. Kouwenhoven, G. de Lange, and A. Kou, Gate-Tunable Field-Compatible Fluxonium, Phys. Rev. Appl. **14**, 064038 (2020).
[35] W. Uilhoorn, J. G. Kroll, A. Bargerbos, S. D. Nabi, C.-K. Yang, P. Krogstrup, L. P. Kouwenhoven, A. Kou, and G. de Lange, Quasiparticle trapping by orbital effect in a hybrid superconducting-semiconducting circuit, arXiv e-prints (2021), ArXiv:2105.11038.
[36] O. O. Otelaja, J. B. Hertzberg, M. Aksit, and R. D. Robinson, Design and operation of a microfabricated phonon spectrometer utilizing superconducting tunnel junctions as phonon transducers, New J. Phys. **15**, 043018 (2013).
[37] W. Eisenmenger and A. H. Dayem, Quantum Generation and Detection of Incoherent Phonons in Superconductors, Phys. Rev. Lett. **18**, 125 (1967).
[38] M. Welte, K. Lassemann, and W. Eisenmenger, Emission of high frequency relaxation phonons by superconducting aluminium tunneling junctions, J. Phys. Colloq. **33**, 25 (1972).
[39] W. Eisenmenger, Superconducting tunneling junctions as phonon generators and detectors, Phys. Acoust. **12**, 79 (1976).
[40] M. Lenander, H. Wang, R. C. Bialczak, E. Lucero, M. Mariantoni, M. Neeley, A. D. O'Connell, D. Sank, M. Weides, J. Wenner, T. Yamamoto, Y. Yin, J. Zhao, A. N. Cleland, and J. M. Martinis, Measurement of energy decay in superconducting qubits from nonequilibrium quasiparticles, Phys. Rev. B **84**, 024501 (2011).
[41] J. Wenner, Y. Yin, E. Lucero, R. Barends, Y. Chen, B. Chiaro, J. Kelly, M. Lenander, M. Mariantoni, A. Megrant, C. Neill, P. J. J. O'Malley, D. Sank, A. Vainsencher, H. Wang, T. C. White, A. N. Cleland, and J. M. Martinis, Excitation of Superconducting Qubits from Hot

Nonequilibrium Quasiparticles, Phys. Rev. Lett. **110**, 150502 (2013).

[42] When quasiparticles recombine, they can also emit photons rather than phonons. However, as the final density of states corresponding to this process is much smaller than the density of states for phonon emission, we neglect this effect.

[43] M. Martinez, L. Cardani, N. Casali, A. Cruciani, G. Pettinari, and M. Vignati, Measurements and Simulations of Athermal Phonon Transmission from Silicon Absorbers to Aluminum Sensors, Phys. Rev. Appl. **11**, 064025 (2019).

[44] L. I. Glazman and G. Catelani, Bogoliubov quasiparticles in superconducting qubits, SciPost Phys. Lect. Notes, 31 (2021).

[45] D. J. van Woerkom, A. Geresdi, and L. P. Kouwenhoven, One minute parity lifetime of a NbTiN Cooper-pair transistor, Nat. Phys. **11**, 547 (2015).

[46] G. Marchegiani, L. Amico, and G. Catelani, Quasiparticles in superconducting qubits with asymmetric junctions, PRX Quantum **3**, 040338 (2022).

[47] L. J. Splitthoff, A. Bargerbos, L. Grünhaupt, M. Pita-Vidal, J. J. Wesdorp, Y. Liu, A. Kou, C. K. Andersen, and B. van Heck, Gate-Tunable Kinetic Inductance in Proximitized Nanowires, Phys. Rev. Appl. **18**, 024074 (2022).

[48] X. Jin, A. Kamal, A. Sears, T. Gudmundsen, D. Hover, J. Miloshi, R. Slattery, F. Yan, J. Yoder, T. Orlando, S. Gustavsson, and W. Oliver, Thermal and Residual Excited-State Population in a 3D Transmon Qubit, Phys. Rev. Lett. **114**, 240501 (2015).

[49] K. Serniak, M. Hays, G. de Lange, S. Diamond, S. Shankar, L. Burkhart, L. Frunzio, M. Houzet, and M. Devoret, Hot Nonequilibrium Quasiparticles in Transmon Qubits, Phys. Rev. Lett. **121**, 157701 (2018).

[50] B. M. Varbanov, F. Battistel, B. M. Tarasinski, V. P. Ostroukh, T. E. O'Brien, L. DiCarlo, and B. M. Terhal, Leakage detection for a transmon-based surface code, npj Quantum Inf. **6**, 102 (2020).

[51] M. McEwen, *et al.*, Removing leakage-induced correlated errors in superconducting quantum error correction, Nat. Commun. **12**, 1761 (2021).

[52] S. B. Kaplan, C. C. Chi, D. N. Langenberg, J. J. Chang, S. Jafarey, and D. J. Scalapino, Quasiparticle and phonon lifetimes in superconductors, Phys. Rev. B **14**, 4854 (1976).

[53] J. G. Kroll, F. Borsoi, K. L. van der Enden, W. Uilhoorn, D. de Jong, M. Quintero-Pérez, D. J. van Woerkom, A. Bruno, S. R. Plissard, D. Car, E. P. A. M. Bakkers, M. C. Cassidy, and L. P. Kouwenhoven, Magnetic-Field-Resilient Superconducting Coplanar-Waveguide Resonators for Hybrid Circuit Quantum Electrodynamics Experiments, Phys. Rev. Appl. **11**, 064053 (2019).

[54] R. Meservey and P. M. Tedrow, Properties of very thin aluminum films, J. Appl. Phys. **42**, 51 (1971).

[55] S. B. Kaplan, Acoustic matching of superconducting films to substrates, J. Low Temp. Phys. **37**, 343 (1979).

[56] J. Wenner, M. Neeley, R. C. Bialczak, M. Lenander, E. Lucero, A. D. O'Connell, D. Sank, H. Wang, M. Weides, A. N. Cleland, and J. M. Martinis, Wirebond crosstalk and cavity modes in large chip mounts for superconducting qubits, Supercond. Sci. Technol. **24**, 065001 (2011).

[57] B. Lienhard, J. Braumuller, W. Woods, D. Rosenberg, G. Calusine, S. Weber, A. Vepsalainen, K. O'Brien, T. P. Orlando, S. Gustavsson, and W. D. Oliver, Microwave packaging for superconducting qubits, 2019 IEEE MTT-S International Microwave Symposium (IMS), 18850626 (2019).

[58] V. Iaia, J. Ku, A. Ballard, C. P. Larson, E. Yelton, C. H. Liu, S. Patel, R. McDermott, and B. L. T. Plourde, Phonon downconversion to suppress correlated errors in superconducting qubits, Nat. Commun. **13**, 6425 (2022).

[59] I. M. Pop, K. Geerlings, G. Catelani, R. J. Schoelkopf, L. I. Glazman, and M. H. Devoret, Coherent suppression of electromagnetic dissipation due to superconducting quasiparticles, Nature **508**, 369 (2014).

[60] A. Gyenis, P. S. Mundada, A. Di Paolo, T. M. Hazard, X. You, D. I. Schuster, J. Koch, A. Blais, and A. A. Houck, Experimental Realization of a Protected Superconducting Circuit Derived from the 0–π Qubit, PRX Quantum **2**, 010339 (2021).

[61] C. Janvier, L. Tosi, L. Bretheau, Ç. O. Girit, M. Stern, P. Bertet, P. Joyez, D. Vion, D. Esteve, M. F. Goffman, H. Pothier, and C. Urbina, Coherent manipulation of Andreev states in superconducting atomic contacts, Science **349**, 1199 (2015).

[62] M. Hays, V. Fatemi, D. Bouman, J. Cerrillo, S. Diamond, K. Serniak, T. Connolly, P. Krogstrup, J. Nygård, A. L. Yeyati, A. Geresdi, and M. H. Devoret, Coherent manipulation of an Andreev spin qubit, Science **373**, 430 (2021).

[63] D. Rainis and D. Loss, Majorana qubit decoherence by quasiparticle poisoning, Phys. Rev. B **85**, 174533 (2012).

[64] T. Karzig, W. S. Cole, and D. I. Pikulin, Quasiparticle Poisoning of Majorana Qubits, Phys. Rev. Lett. **126**, 057702 (2021).

[65] G. J. Schinner, H. P. Tranitz, W. Wegscheider, J. P. Kotthaus, and S. Ludwig, Phonon-Mediated Nonequilibrium Interaction between Nanoscale Devices, Phys. Rev. Lett. **102**, 186801 (2009).

[66] G. Granger, D. Taubert, C. E. Young, L. Gaudreau, A. Kam, S. A. Studenikin, P. Zawadzki, D. Harbusch, D. Schuh, W. Wegscheider, Z. R. Wasilewski, A. A. Clerk, S. Ludwig, and A. S. Sachrajda, Quantum interference and phonon-mediated back-action in lateral quantum-dot circuits, Nat. Phys. **8**, 522 (2012).

[67] C. W. J. Beenakker, Universal Limit of Critical-Current Fluctuations in Mesoscopic Josephson Junctions, Phys. Rev. Lett. **67**, 3836 (1991).

[68] E. M. Spanton, M. Deng, S. Vaitiekėnas, P. Krogstrup, J. Nygård, C. M. Marcus, and K. A. Moler, Current-phase relations of few-mode InAs nanowire Josephson junctions, Nat. Phys. **13**, 1177 (2017).

[69] K. Zuo, V. Mourik, D. B. Szombati, B. Nijholt, D. J. van Woerkom, A. Geresdi, J. Chen, V. P. Ostroukh, A. R. Akhmerov, S. R. Plissard, D. Car, E. P. Bakkers, D. I. Pikulin, L. P. Kouwenhoven, and S. M. Frolov, Supercurrent Interference in Few-Mode Nanowire Josephson Junctions, Phys. Rev. Lett. **119**, 187704 (2017).

[70] J. Heinsoo, C. K. Andersen, A. Remm, S. Krinner, T. Walter, Y. Salathé, S. Gasparinetti, J.-C. Besse, A. Potočnik, A. Wallraff, and C. Eichler, Rapid High-Fidelity Multiplexed

Readout of Superconducting Qubits, Phys. Rev. Appl. **10**, 034040 (2018).

[71] A. Kringhøj, L. Casparis, M. Hell, T. W. Larsen, F. Kuemmeth, M. Leijnse, K. Flensberg, P. Krogstrup, J. Nygård, K. D. Petersson, and C. M. Marcus, Anharmonicity of a superconducting qubit with a few-mode Josephson junction, Phys. Rev. B **97**, 060508(R) (2018).

[72] S. Hart, Z. Cui, G. Ménard, M. Deng, A. E. Antipov, R. M. Lutchyn, P. Krogstrup, C. M. Marcus, and K. A. Moler, Current-phase relations of InAs nanowire Josephson junctions: From interacting to multimode regimes, Phys. Rev. B **100**, 064523 (2019).

[73] A. Bargerbos, W. Uilhoorn, C.-K. Yang, P. Krogstrup, L. P. Kouwenhoven, G. de Lange, B. van Heck, and A. Kou, Observation of Vanishing Charge Dispersion of a Nearly Open Superconducting Island, Phys. Rev. Lett. **124**, 246802 (2020).

[74] A. Kringhøj, B. van Heck, T. W. Larsen, O. Erlandsson, D. Sabonis, P. Krogstrup, L. Casparis, K. D. Petersson, and C. M. Marcus, Suppressed Charge Dispersion via Resonant Tunneling in a Single-Channel Transmon, Phys. Rev. Lett. **124**, 246803 (2020).

[75] 4TU.ResearchData at doi:10.4121/c.6076814